

Citation for published version:

Ferrara, C, Eames, C, Islam, MS & Tealdi, C 2016, 'Lattice strain effects on doping, hydration and proton transport in scheelite-type electrolytes for solid oxide fuel cells', *Physical Chemistry Chemical Physics*, vol. 18, no. 42, pp. 29330-29336. <https://doi.org/10.1039/c6cp06395k>

DOI:

[10.1039/c6cp06395k](https://doi.org/10.1039/c6cp06395k)

Publication date:

2016

Document Version

Peer reviewed version

[Link to publication](#)

University of Bath

Alternative formats

If you require this document in an alternative format, please contact:
openaccess@bath.ac.uk

General rights

Copyright and moral rights for the publications made accessible in the public portal are retained by the authors and/or other copyright owners and it is a condition of accessing publications that users recognise and abide by the legal requirements associated with these rights.

Take down policy

If you believe that this document breaches copyright please contact us providing details, and we will remove access to the work immediately and investigate your claim.

Lattice strain effects on doping, hydration and proton transport in scheelite-type electrolytes for solid oxide fuel cells

Chiara Ferrara,^a Chris Eames,^b M. Saiful Islam,^b Cristina Tealdi^{a,*}

Received 00th January 20xx,
Accepted 00th January 20xx

DOI: 10.1039/x0xx00000x

www.rsc.org/

Lattice strain is considered a promising approach to modulating the structural and functional properties of oxide materials. In this study we investigate the effect of lattice strain on doping, hydration and proton transport for the family of scheelite-type proton conductors using both atomistic and DFT computational methods. Results suggest that tensile strain improves the dopant solubility and proton uptake of the material. The anisotropic proton pathways change from being within the *a-b* plane to being in the *a-c* plane. However, the predicted reduction in migration barrier suggests that improvements in ionic conductivity due to lattice strain effects will be limited, in contrast with the work on oxide ion conduction. Such results are rationalized in terms of structural changes and differences in migration steps between oxide ions and protonic species.

1. Introduction

Proton conducting oxides have received considerable attention over the past decades in view of their potential to lower the Solid Oxide Fuel Cell (SOFC) operating temperature to an intermediate-to-low temperature range.^{1–3} Such a decrease in the operating temperature would improve the chemical and mechanical stability of the SOFCs and reduce their cost. Decreasing the operating temperature while maintaining the high ionic conductivity target of the electrolyte layer (10^{-2} S cm⁻¹) and the rapid surface oxygen exchange kinetics at the cathode requires the development of novel functional materials or a significant optimization of the existing systems.⁴

With regard to the electrolyte layer, the reference class of compounds for proton conducting SOFCs is the family of doped perovskites with general formula ABO₃ (A=Ca, Sr, Ba; B=Ce, Zr). Proton conduction in this system was reported during the 1980's by Iwahara et al.⁵, with conductivities achieving 0.01 S cm⁻¹ at 400°C for doped BaZrO₃.⁶ Major problems associated with the use of perovskite-type proton conductors are the low chemical stability in CO₂ containing atmosphere and the difficult sinterability.² To overcome this drawback, several classes of oxides have been proposed.^{1,7}

One of the latest family of oxides proposed is the ortho-niobates and ortho-tantalates class of compounds with general

formula LnXO₄ (Ln rare earth, X = Nb, Ta).^{8,9} This family of oxides is characterized by the presence of a phase transition between the low temperature fergusonite-type structure and the high temperature scheelite-type polymorph.¹⁰ The best reported conductivity values are obtained for the 1% Ca doped LaNbO₄ composition, reaching reasonable values of 10^{-3} S cm⁻¹ at 950°C in wet atmosphere.⁸

Different strategies have been proposed for further improvement of the transport properties of these ortho-niobates. As the conductivity depends on the concentration of the charge carriers, different dopants were tested but the solubility limit for Ca²⁺ on the La³⁺ site is found to be in the 0.5–1.0% range.¹¹ Doping on the B site was also considered, but the dopant solubility is also low and in general the activation barrier for proton migration for the B-site doped materials is higher than the A-site doped systems.¹² Therefore, although several compositions and combinations of dopants were considered, no dramatic improvement of the ionic conductivity was achieved.^{7,13–17} This “chemical approach”, based on the search for novel compositions or better dopants, has represented the driving path for the optimization of the transport properties of ionic conducting materials for decades.

A more “physical approach”, based on the exploitation of lattice strain effects on the transport properties of ionic conducting materials, is currently acquiring growing interest.¹⁸ In this regard, computational and experimental studies have focused on electrolytes^{19–22} as well as cathode materials^{23,24} for SOFCs based on oxide-ion conduction. In general, it has been shown that lattice strain effects can improve the transport properties of oxide ion conductors by several orders of magnitude, as a consequence of structural modifications. For example, computational studies on the fluorite-structure oxide ion conductors have suggested the possibility to increase

^a Department of Chemistry, University of Pavia and INSTM, Viale Taramelli 16, 27100 Pavia, Italy.

^b Department of Chemistry, University of Bath, Bath, BA2 7AY, UK.

* Corresponding author: cristina.tealdi@unipv.it

Electronic Supplementary Information (ESI) available: [Table of potential parameters, calculated density of states and energy barriers profile obtained from NEB calculation]. See DOI: 10.1039/x0xx00000x

the ionic conductivity by a factor of 10^4 – 10^6 within the strained system,^{19,20} and thin films of $\text{La}_{0.6}\text{Sr}_{0.4}\text{CoO}_{3-6}$ have been reported with oxygen diffusivity values of two orders of magnitude higher compared to the bulk material.²³ Similar promising results have been obtained and predicted for K_2NiF_4 -type cathode materials²⁵ and perovskite-type electrolytes.²¹ In contrast, the same approach has received very limited attention in the field of proton conducting SOFCs, with a computational study devoted to the investigation of biaxial strain effects on the proton conductivity of Y-doped BaZrO_3 through reactive molecular dynamics.²⁶ This study suggests that moderate biaxial strain can slightly improve proton diffusivity in perovskite-type materials.

In this work, we present a computational investigation of the influence of biaxial strain on dopant solubility, hydration energetics and proton migration for the scheelite-type LaNbO_4 system. The application of biaxial strain mimics the situation of strained epitaxial films where the strain is induced by a lattice mismatch at the interface with the substrate. The results presented are therefore relevant to the preparation of micro-SOFCs. In addition, this study aims to expand the set of systems explored in the application of strain engineering as a strategy to modulate the functional properties of materials in solid state thin film devices.

2. Computational methods

The atomistic energy minimization and DFT methods employed in this study have been presented extensively elsewhere.^{27,28} In this study static lattice simulations were performed according to the energy minimization procedure embodied in the GULP code.²⁹ The interaction between ions was modelled with Buckingham pair potentials. Electron polarizability was described by the shell model.³⁰ Lattice relaxation after the introduction of a charged point defect was treated according to the Mott-Littleton method.³¹ The set of potential parameters used in this study (Table S1 of the ESI) was already optimized and used for the description of the tetragonal unstrained LaNbO_4 system.³² The O-H interaction has been described with the use of the well-established Morse potential (Table S2 in the ESI) already used in other proton conducting oxides.^{33–35} Within the GULP code, lattice strain in the -3% – +3% range of the unstrained relaxed cell parameters was applied simultaneously along the *a* and *b* directions while the third cell parameter and all the atomic coordinates were allowed to relax. Calculations were performed in the *P1* space group, to allow for possible lowering of the symmetry upon the imposition of lattice strain.

The DFT-based calculations were performed with the VASP code³⁶ using projector augmented wave (PAW) pseudopotentials and the PBE exchange correlation functional term proposed by Perdew et al.³⁷ The energy cut-off was set at 600 eV and the unit cells (both strained and unstrained) were optimized until the residual forces were less than $0.005 \text{ eV } \text{\AA}^{-1}$ and the total energy difference less than 0.005 eV using an $8 \times 8 \times 4$ k-point grid. In this case, for the strained systems, -3% and +3% strain compared to the relaxed lattice parameters for

the unstrained system were applied simultaneously along the *a* and *b* directions. Full relaxation of the atomic coordinates was then achieved for different values of the *c* lattice parameter, so as to find the one associated to a minimum in the total energy of the unit cell (see Figure S1-ESI for details). The energetics of proton transport were calculated using the DFT-based Nudged Elastic Band (NEB) method. For these NEB calculations, $2 \times 2 \times 1$ supercells containing a single proton were employed. The NEB calculations were performed using the climbing image method³⁸ and considering different number of images according to the complexity of the migration paths. The k-point grid was reduced to $2 \times 2 \times 2$ while maintaining the energy cut-off at 600 eV.

3. Results and discussion

3.1 Structural modelling

The tetragonal scheelite-type structure of LaNbO_4 (space group *I4*/1a), presented in Figure 1, consists of isolated NbO_4 tetrahedral units separated by La^{3+} ions.

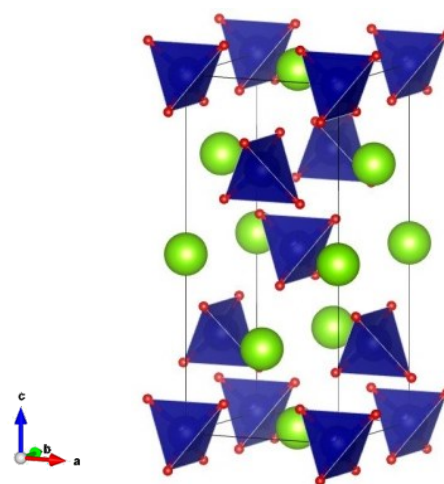


Figure 1 – Scheelite crystal structure of LaNbO_4 . Nb^{5+} (blue) ions are forming NbO_4 units separated along the three dimensions by La^{3+} (green) ions in four-fold coordination with oxygen (red).

We first turn our attention to the effect of applied strain on the scheelite structure. Figure 2 shows the calculated volume and lattice parameters as positive and negative strains are applied. In general, and as usually observed for oxide materials, as a positive strain is applied biaxially in the *a*-*b* plane the *c* lattice parameter is observed to contract whereas overall the volume slightly increases. When negative strain is applied the *c* lattice parameter increases but the volume slightly decreases. We note the excellent agreement between the unstrained experimental lattice parameters and volume and those calculated by both computational techniques. Furthermore, both computational techniques show the same magnitude of *c* parameter variation as strain is applied. All of this supports the validity of the models and the stability of the structure under the applied strain conditions.

Structural analysis of the calculated results indicates that when the strain is applied in the *a*-*b* plane the tetragonal

symmetry is maintained and the NbO_4 tetrahedra are undistorted; the Nb-O bond lengths respond linearly to the applied strain (see Figure S3-ESI). Since Nb^{5+} has a d^0 electronic structure there are no crystal field or magnetic effects to encourage asymmetric distortions of the tetrahedra. In addition, the density of states (DOS) obtained from our DFT calculations are in good agreement with the DOS previously reported for the same structure when no strain is applied³⁹ (Figure S2 of the ESI).

(110)-oriented NdGaO_3 has been reported.⁴² In this case, a decrease of transition temperature of more than 200°C compared to the corresponding bulk system was reported, supporting a considerable reduction of the monoclinic distortion in the epitaxial films. These results suggest that with the right combination of substrate type and deposition conditions it is possible to deposit epitaxial scheelite-type strained films. For these reasons this study focuses on the tetragonal scheelite-type polymorph.

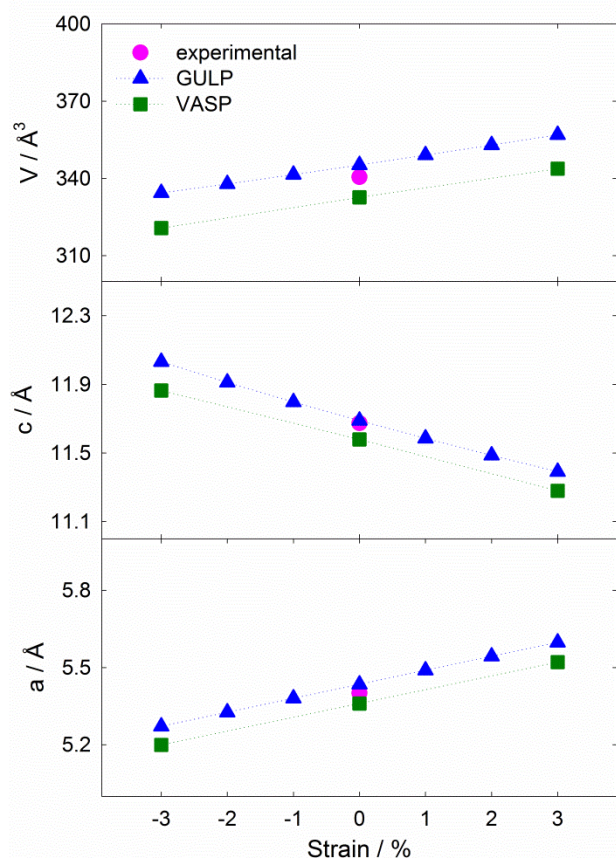
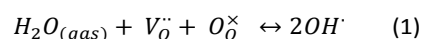


Figure 2 – Experimental⁴⁰ and calculated structural parameters and cell volume for the tetragonal LaNbO_4 structure under various applied biaxial strains in the a - b plane.

We recall that the LaNbO_4 system is characterized by a phase transition between a monoclinic room temperature fergusonite-type structure and a tetragonal high temperature scheelite-type structure around 500°C.¹⁰ As the high temperature phase is the best proton conductor, low-temperature stabilization of the scheelite phase is desirable. In addition, the presence of a phase transition within the operating temperature regime is always considered detrimental for practical applications. Successful results have been recently reported for the room temperature deposition of $\text{La}_{0.99}\text{Ca}_{0.01}\text{NbO}_4$ films with the scheelite structure.⁴¹ The inversion of the phase stability between the fergusonite and the scheelite polymorphs has been ascribed in that case to the nanostructured nature of the film in combination with a suitable substrate. At the same time, the deposition of epitaxial fergusonite-type films of $\text{La}_{0.995}\text{Ca}_{0.005}\text{NbO}_{4-\delta}$ by PLD on

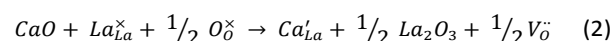
3.2 Hydration and Ca-doping

The mechanism through which protons are introduced in an oxide structure is accepted to be substantially the same for all host systems.^{43,44} Oxides can accommodate a certain concentration of protons *via* the incorporation of H^+ ions generated by the dissociative absorption of water molecules from the gas phase. The OH^- group can fill an oxygen vacancy, while the H^+ ion obtained from the dissociation directly bonds to a lattice oxygen position. The overall reaction can be expressed in Equation 1, using Kröger-Vink notation, as:



Strain may affect the energetics of proton incorporation. To test this, we have calculated the hydration enthalpy as a function of strain according to Equation 1, and the results are shown in Figure 3. The hydration enthalpy shows a clear decrease with increasing strain, suggesting a positive effect of tensile strain on the amount of water incorporation within the system. This trend reflects the changes in the formation energies of the OH group and the oxygen vacancies, both of which become more favourable as tensile strain is applied (Figure S4-ESI). Such changes in defect formation energy reflect structural rearrangements due to the presence of defects.

The presence of oxygen vacancies in the crystal is generally obtained through doping with acceptor dopant species. For LaNbO_4 , the most successful way to introduce oxygen vacancies that can be filled by protonic species is the substitution of La^{3+} with Ca^{2+} ,^{9,11} according to the following equation:



However, the low solubility of dopant ions experimentally observed in the scheelite structure prevents any conductivity enhancement through doping.^{11,45} In our study, in order to determine if the application of strain improves the solubility of dopants, we have evaluated the solution energies of Ca^{2+} in LaNbO_4 as a function of the imposed strain. The calculated solution energy decreases with the applied strain, from 1.25 eV for the unstrained system to 1.05 eV for the 3% tensile strained system. Such a decrease in solution energy suggests that it is possible to dope a higher concentration of Ca^{2+} into tensile strained crystals, which would enhance the proton transport properties of scheelite LaNbO_4 .

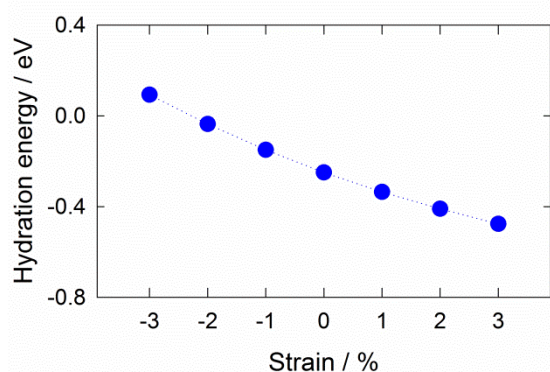


Figure 3 – Calculated hydration energies as a function of applied strain.

Another important aspect of extrinsic doping is the possibility of binding of dopant ions to mobile defects. Due to their opposite charge, oxygen vacancies introduced by the extrinsic doping can associate with the dopant ions, forming a cluster; this effect has been widely observed and described for oxygen conductor materials.⁴⁶ Dopant ions can also trap migrating proton species.⁴³ The clustering effect in Ca-doped LaNbO_4 has been evaluated by comparing the energy of the simple bi-component cluster system where the M' ion is placed in the first coordination sphere of the $\text{V}_{\text{O}}^{\bullet\bullet}$ (or the OH^\bullet group) and the sum of the corresponding isolated defects according to the formula:

$$E_{\text{bind}} = E_{\text{cluster}} - \sum E_{\text{isol.def.}} \quad (3)$$

With this convention, negative values of binding energy imply that the dopants and defects are bound and the cluster is more stable than the isolated defects. This approach has been widely applied to the estimation of binding energy terms for oxide ion and proton conducting oxides, successfully reproducing experimental trends in their conduction properties.⁴⁷ Our calculations show that strain lowers the binding energy of defect clusters; the binding energy of the $\text{Ca}^{2+}\text{-OH}^\bullet$ pair cluster reduces from -0.25 eV for the unstrained system to -0.18 eV for the 3% tensile strained system. Similarly, the Ca^{2+} -oxygen vacancy pair cluster is predicted to be less bound in the 3% tensile strained system, with binding energies lowered from -0.91 eV to -0.77 eV.

The formation of a cluster involving a mobile defect leads to an increase of the migration barrier. Binding energies between dopants ion and protonic species are therefore considered detrimental for application since they reduce proton mobility in the system.^{43,48} At the same time, trapping of the oxygen vacancies is expected to decrease the proton concentration, by adding an energy term to the enthalpy of hydration.⁴³ The predicted lowering of the binding energy effects in tensile strained LaNbO_4 suggests a higher mobility of the proton species if tensile strain is applied, together with an easier incorporation of protonic species in the system. We note that such trapping effects are observed experimentally for high doping levels. As the experimental solubility limit of

the dopants in the scheelite structure is very low, the clustering effect might be less significant in this system.

3.3 Proton positions and migration paths

Proton species in oxides are usually found near the oxygen ions, as part of a hydroxyl group. For this reason, different positions around the unique oxygen crystallographic site of the LaNbO_4 structure have been explored using DFT. Two distinct sites (labelled H_1 and H_2 , see Fig. 4) arise as the most favourable, in agreement with previous reports for the unstrained system.⁴⁹ The stable proton positions were also evaluated for the +3 and -3% strained cells, in order to see if the relative stability of the two positions is affected by applied strain, as shown in Table 1.

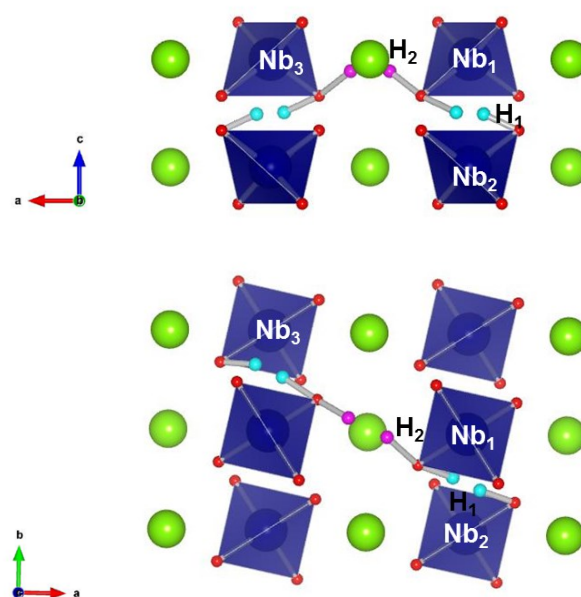


Figure 4 – Stable proton sites in scheelite LaNbO_4 - H_1 (cyan) and H_2 (pink) around the NbO_4 tetrahedra (blue, La ions in green). H_1 is more favourable than H_2 in the unstrained crystal.

In the H_1 site the proton is bonded to the O of the Nb_1 site and the O-H bond is directed towards the oxygen ion of the nearest NbO_4 units found along the c axis (Nb_2 in Figure 4) and is further stabilized by hydrogen bonds. By contrast, in the H_2 site the O-H bond points in the direction of the nearest La ions along the a axis, in the direction of the next neighbour NbO_4 unit within the a - b plane (Nb_3 in Figure 4). The position of these two sites remains largely unaffected by the application of the strain, although strain does significantly alter their relative energies, as shown in Table 1. For the negatively strained cell the H_1 site is the most stable position but the energy difference decreases linearly with applied strain so that the two positions are energetically equivalent in the tensile strained system. In all cases the O-H distance is found to be 0.98-1.00 Å, as usually observed in oxides. The presence of stable proton sites at ~ 1 Å around the oxygen position has been predicted and observed in LaNbO_4 as well as in other proton conductor materials.^{49–51}

Table 1 – Energy differences between H₁ and H₂ proton positions as function of the applied strain.

Strain	E(H ₂)-E(H ₁) /eV
-3 %	0.23
0	0.15
+3 %	0.04

Starting from these two favourable proton sites, several proton migration routes can be considered. Previous studies on proton conducting oxides have established that the diffusion mechanism is based on two different mechanisms: proton hopping between two distinct oxygen sites and rotation of the proton ion around an oxygen position. For the scheelite structure four pathways for proton migration between sites are possible, shown in figure 5; (i) inter-tetrahedral hops between H₁-sites in the **a** or **b** directions, (ii) inter-tetrahedral hops between H₂-sites in the **a** or **b** directions, (iii) migration from a H₁ site to a H₂ site (or vice versa) *via* rotation of the O-H bond around the tetrahedral edge (iv) inter-tetrahedral hops between H₁ and H₂ sites in the **c** direction.

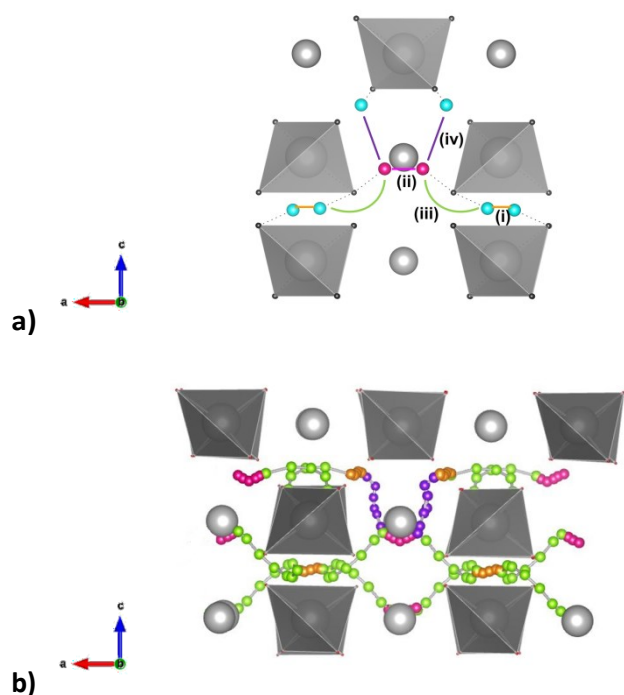


Figure 5 – (a) Schematic representation of the stable proton positions in the tetragonal LaNbO₄ structure; NbO₄ tetrahedral units in grey, La ions in light grey. The two proton positions are differentiated with colors: H₁ in light blue, H₂ in pink. (b) Pathways calculated using the DFT-based nudged elastic band method. Colors indicate distinct proton migration events; (i) Hops between adjacent H₁ sites in orange, (ii) hops between adjacent H₂ sites in pink, jumps between H₁ and H₂ sites in violet, rotations around the same oxygen ion from H₁ to H₂ position in green. A combination of (i), (ii) and (iii) results in long range migration in the **a-b** plane while migration along the **c** axis requires step (iv).

In a previous computational study on unstrained scheelite LaNbO₄, Fjeld and coworkers found that protons diffuse preferentially in the **a-b** plane.⁴⁹ Proton transfer between H₁ or H₂ sites (type i or ii migration) was calculated to have very low energy barriers (0.04-0.08 eV). The rate determining step for the migration within the **a-b** plane was found to be the complex type iii migration from a H₁ site to a H₂ site involving a combination of rotation and hopping, with an energy barrier of 0.41 eV. Diffusion along the **c** axis *via* a type iv jump between H₁ and H₂ sites was found to be very unfavourable, with a much larger activation barrier of 0.74 eV, suggesting strongly anisotropic behaviour with negligible proton conduction in the **c** direction.

Given that strain alters both the **c** parameter (and as a result the proton site-site hopping distances) and the proton site energies, it is possible that the proton migration will also be affected by the application of strain. To investigate this we calculated the proton migration energies for all four paths for both strained and unstrained cells (Figure 6).

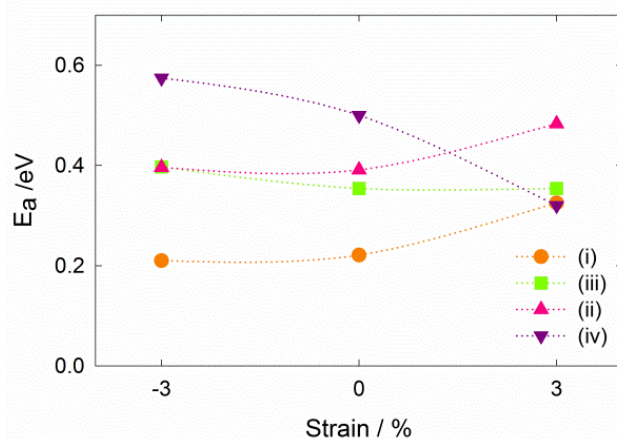


Figure 6 - Energy barriers derived from NEB calculations for the migration steps schematically represented in Figure 5 referenced with the same labels and color scheme. Migration profiles are reported in Fig S5-ESI.

First, for unstrained cells, we find the same trend as Fjeld et al. discussed above;⁴⁹ a large migration energy along the **c**-direction of 0.51 eV (type iv), relatively low migration energy for equivalent site hops (type i and ii) and a rate limiting migration energy in the **a-b** plane of approximately 0.4 eV (type iii). Differences between the calculated values can be ascribed to our use of a more accurate basis set, spin polarization to capture the energetics of unpaired electrons during bond breaking and more images along the NEB path. Nevertheless, the overall prediction remains consistent: anisotropic migration confined to the **a-b** plane. Second, for cells compressively strained we find that there is little change for the migration energies in the **a-b** plane but the migration barrier in the **c**-direction increases from 0.51 eV to 0.57 eV. Overall, compressive strain would not be expected to impact the proton conductivity other than to exacerbate the already high degree of anisotropy. Finally, we consider tensile strain. It can be seen in Figure 6 that there is a significant reduction in

the migration barrier along the c -direction from 0.51 eV to 0.32 eV (type iv migration). The rate limiting migration barrier in the a - b plane (type ii hop) increases markedly from 0.39 eV to 0.48 eV. These changes in activation energy can be rationalized by the fact that tensile strain increases the proton site to site distance in the a - b plane and reduces it in the c -direction. The overall effect of tensile strain is to maintain the anisotropic proton diffusion, but to switch it from the a - b plane to the a - c plane, as represented schematically in Figure 7.

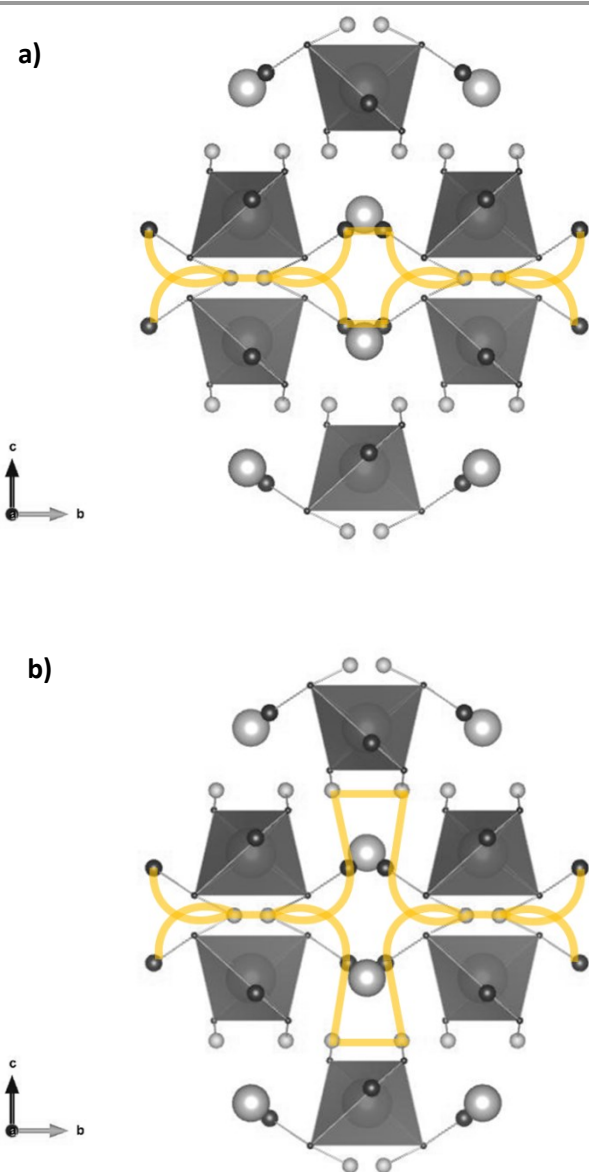


Figure 7 – Schematic representation of long range proton diffusion pathways in (a) unstrained and (b) tensile strained LaNbO_4 . (NbO_4 tetrahedra - dark grey, La^{3+} - large light grey spheres, H_1 - small light grey spheres, H_2 small dark grey spheres, proton migration pathway - orange).

Further atomic-scale analysis reveals that proton migration is accompanied by local rearrangement of the structure involving tilting, rotation or distortion of polyhedra. For the unstrained system, the proton hopping between two H_1 sites

presents the lowest activation energy ~ 0.2 eV. By contrast hopping between H_2 sites has a two times higher energy barrier ~ 0.4 eV; this difference can be explained by considering the local O-H bonds along the two migration steps. At the saddle point for the H_1 - H_1 hop the O-H distances from the initial and final oxygen sites are 1.24 Å and 1.23 Å, whereas for H_2 - H_2 hops the O-H distances at the saddle point are 1.55 Å and 1.53 Å respectively. The increase in the O-H distance and the formal breaking of the O-H bond in H_2 - H_2 hops requires a higher energy. Strain alters these energy barriers since it alters the proton site to site distances and directly affects the extent to which the O-H bonds are broken. Further support for this comes from the fact that the 0.36 eV rotational energy barrier around the NbO_4 tetrahedra (migration step iii of Figure 5) is not altered by strain; it does not involve bond breaking and does not involve a change in site to site distances.

Experimentally reported values of migration barrier for proton conductivity in bulk scheelite-type Ca-doped LaNbO_4 are close to 0.5 eV,^{11,45} in agreement with the values obtained in this study for the unstrained system. Further studies are needed to investigate how extended defects such as dislocations, grain boundaries and space charge regions contribute to the experimentally observed conductivity increase in strained thin films of Ca-doped LaNbO_4 .⁴² We recall that in the Y-doped BaZrO_3 proton conductor, it was predicted computationally that lattice strain effects could only account for a limited increase in conductivity.²⁶ However, epitaxial thin films of Y-doped BaZrO_3 presented major improvement in conductivity compared to the bulk material;⁵² such an effect was attributed to the considerable reduction of the grain boundary resistivity in epitaxial strained thin films compared to bulk materials.

4. CONCLUSIONS

Previous attempts to try and improve the proton conductivity of scheelite-type LaNbO_4 have focused on doping strategies to increase the oxygen vacancy concentration and thereby the uptake of protonic species, but have proved ineffective due to the inherently low dopant solubility. Prompted by the growing interest in lattice strain effects on the properties of a wide range of materials, here we used computational methods to characterize how strain applied to the LaNbO_4 SOFC electrolyte material affects the doping, defect and proton transport properties.

Four main points emerge:

1. Tensile strain in the a - b plane improves the solubility for Ca^{2+} dopants which increases the number of oxygen vacancies, allowing more protons to be accommodated by the structure. The hydration energy is reduced which should further increase proton uptake. Binding energies of extrinsic defects are lower in strained crystals and might result in less trapping of protons by defect clusters.
2. Tensile strain makes the two most stable proton sites in the structure energetically degenerate and equally likely to be occupied.
3. The anisotropic proton pathways alter from being in the a - b plane to being in the a - c plane. This change is rationalized by

the reduction in the c -lattice parameter and the proton hopping distance as a - b strain is applied. A small reduction in the migration barrier for the rate determining step is predicted.

4. Compressive strain has the opposite effect on these properties to tensile strain. It reduces dopant solubility, site degeneracy and makes proton migration more anisotropic and should be avoided.

Our results suggest that the application of lattice strain should be regarded as an effective strategy to modulate transport properties where site to site hopping is crucial to conduction (i.e. oxide ion or alkali ion conductors). Where proton transport in oxide materials usually requires both site to site hopping and rotation around oxygen sites, the structural modifications induced by lattice strain may not be as effective in the modulation of transport properties.

Acknowledgements

We gratefully acknowledge support from the EPSRC for the Energy Materials Programme grant (EP/K016288), Archer HPC facilities through the Materials Chemistry Consortium (EP/L000202) and the Italian Ministry of Education, University and Research (MIUR) for the FIRB "Futuro in Ricerca" project INCYPIT (RBFR12CQP5).

References

- 1 E. Fabbri, D. Pergolesi and E. Traversa, *Chem. Soc. Rev.*, 2010, **39**, 4355–4369.
- 2 K. D. Kreuer, *Annu. Rev. Mater. Res.*, 2003, **33**, 333–359.
- 3 L. Malavasi, C. A. J. Fisher and M. S. Islam, *Chem. Soc. Rev.*, 2010, **39**, 4370–4387.
- 4 D. J. Brett, A. Atkinson, N. P. Brandon and S. J. Skinner, *Chem. Soc. Rev.*, 2008, **37**, 1568–1578.
- 5 N. M. H. Iwahara, T. Esaka, H. Uchida, *Solid State Ionics*, 1981, **3**, 359–363.
- 6 K. D. Kreuer, S. Adams, W. Münch, A. Fuchs, U. Klock and J. Maier, *Solid State Ionics*, 2001, **145**, 295–306.
- 7 A. Magrasò, M. L. Fontaine, Y. Larring, R. Bredesen, G. E. Syvertsen, H. L. Lein, T. Grande, M. Huse, R. Strandbakke, R. Haugrud and T. Norby, *Fuel Cells*, 2011, **11**, 17–25.
- 8 R. Haugrud and T. Norby, *Solid State Ionics*, 2006, **177**, 1129–1135.
- 9 R. Haugrud and T. Norby, *Nat Mater*, 2006, **5**, 193–196.
- 10 M. Huse, A. W. B. Skilbred, M. Karlsson, S. G. Eriksson, T. Norby, R. Haugrud and C. S. Knee, *J. Solid State Chem.*, 2012, **187**, 27–34.
- 11 Z. Bi, J. Pena-Martínez, J. H. Kim, C. A. Bridges, A. Huq, J. P. Hodges and M. P. Paranthaman, *Int. J. Hydrogen Energy*, 2012, **37**, 12751–12759.
- 12 A. D. Brandao, J. Gracio, G. C. Mather, V. V. Kharton and D. P. Fagg, *J. Solid State Chem.*, 2011, **184**, 863–870.
- 13 M. Ivanova, S. Ricote, W. A. Meulenbergh, R. Haugrud and M. Ziegner, *Solid State Ionics*, 2012, **213**, 45–52.
- 14 Y. Cao, N. Duan and D. Yan, *J. Solid State Chem.*, 2016, **237**, 248–253.
- 15 S. Wachowski, A. Mielewczyk-Gryn, K. Zagórski, C. Li, P. Jasiński, S. J. Skinner, R. Haugrud and M. Gazda, *J. Mater. Chem. A*, 2016, **11696**–11707.
- 16 L. Xiao, D. Mei, M. Cao, D. Qu and B. Deng, *J. Alloys Compd.*, 2015, **627**, 455–462.
- 17 Y. Cao, N. Duan, X. Wang, B. Chi, L. Jian, JianPu and L. Jian, *J. Eur. Ceram. Soc.*, 2015, **35**, 1979–1983.
- 18 K. Wen, W. Lv and W. He, *J. Mater. Chem. A*, 2015, **3**, 20031–20050.
- 19 A. Kushima and B. Yildiz, *J. Mater. Chem.*, 2010, **20**, 4809.
- 20 R. A. De Souza, A. Ramadan, S. Hörner and S. Hoerner, *Energy Environ. Sci.*, 2012, **5**, 5445.
- 21 C. Tealdi and P. Mustarelli, *J. Phys. Chem. C*, 2014, **118**, 29574–29582.
- 22 N. Schichtel, C. Korte, D. Hesse and J. Janek, *Phys. Chem. Chem. Phys.*, 2009, **11**, 3043–348.
- 23 H.-I. Ji, J. Hwang, K. J. Yoon, J.-W. Son, B.-K. Kim, H.-W. Lee and J.-H. Lee, *Energy Environ. Sci.*, 2013, **6**, 116.
- 24 M. Kubicek, Z. Cai, W. Ma, B. Yildiz, H. Hutter and J. Fleig, *ACS nano*, 2013, 3276–3286.
- 25 N. Tsvetkov, Q. Lu, Y. Chen and B. Yildiz, *ACS Nano*, 2015, **9**, 1613–1621.
- 26 A. Ottocian, G. Dezanneau, C. Gilles, P. Raiteri, C. Knight and J. D. Gale, *J. Mater. Chem. A*, 2014, **2**, 3127.
- 27 R. Catlow, R. Bell, F. Cora, S. a. French, B. Slater and A. Sokol, *Annu. Reports Sect. 'A' Inorganic Chem.*, 2005, 513–547.
- 28 A. Walsh, A. A. Sokol and C. R. A. Catlow, Eds., *Computational Approaches to Energy Materials*, Wiley, 2013.
- 29 J. D. Gale, *J. Chem. Soc., Faraday Trans.*, 1997, **93148**, 629–637.
- 30 B. G. Dick, a. W. Overhauser and A. Jr, BG Dick, Overhauser, *Phys. Rev.*, 1958, **112**, 90–103.
- 31 N. F. Mott and M. J. Littleton, *Trans. Faraday Soc.*, 1938, **34**, 485–499.
- 32 G. C. Mather, C. A. J. Fisher and M. S. Islam, *Chem. Mater.*, 2010, **22**, 5912–5917.
- 33 P. Saul, C. R. A. Catlow and J. Kendrick, *Philosophical Mag. B*, 1985, **51**, 107–117.
- 34 S. J. Stokes and M. S. Islam, *J. Mater. Chem.*, 2010, **20**, 6258.
- 35 S. Phadke, J. C. Nino and M. S. Islam, *J. Mater. Chem.*, 2012, 25388–25394.
- 36 P. E. Blöchl, *Phys. Rev. B*, 1994, **50**, 17953–17979.
- 37 J. P. Perdew and A. Zunger, *Phys. Rev. B*, 1981, **23**, 5048–5079.
- 38 J. Henkelman, P. B. Uberuaga and H. Johansson, *J. Chem. Phys.*, 2000, **113**, 9901.
- 39 A. Kuwabara, R. Haugrud, S. Stølen and T. Norby, *Phys. Chem. Chem. Phys.*, 2009, **11**, 5550–5553.
- 40 W. I. F. David, *Mater. Res. Bull.*, 1983, **18**, 749–756.
- 41 C. Tealdi, E. Quartarone, P. Mustarelli and L. Malavasi, *Nanoscale*, 2015, **7**, 2221–4.
- 42 A. Cavallaro, C. Solís, P. R. Garcia, B. Ballesteros, J. M. Serra and J. L. Santiso, *Solid State Ionics*, 2012, **216**, 25–30.
- 43 T. Norby, M. Widerøe, R. Glöckner and Y. Larring, *Dalt. Trans.*, 2004, 3012–3018.
- 44 K. . Kreuer, *Solid State Ionics*, 1997, **97**, 1–15.
- 45 M. Huse, T. Norby and R. Haugrud, *Int. J. Hydrogen Energy*, 2012, **37**, 8004–8016.
- 46 J. A. Kilner, *Solid State Ionics*, 2000, **129**, 13–23.
- 47 M. S. Islam and R. A. Davies, *J. Mater. Chem.*, 2004, **14**, 86.
- 48 J. A. Dawson and I. Tanaka, *J. Mater. Chem. A*, 2015, **3**, 10045–10051.
- 49 H. Fjeld, K. Toyoura, R. Haugrud and T. Norby, *Phys. Chem. Chem. Phys.*, 2010, **12**, 10313–9.
- 50 K. Toyoura, N. Hatada, Y. Nose, I. Tanaka, K. Matsunaga and T. Uda, *J. Phys. Chem. C*, 2012, **116**, 19117–19124.
- 51 K. Nomura and H. Kageyama, *Solid State Ionics*, 2014, **262**, 841–844.
- 52 D. Pergolesi, E. Fabbri, A. D'Epifanio, E. Di Bartolomeo, A. Tebano, S. Sanna, S. Licoccia, G. Balestrino and E. Traversa, *Nat. Mater.*, 2010, **9**, 846–852.